Journal of Non-Newtonian Fluid Mechanics 322 (2023) 105131

Contents lists available at ScienceDirect

Journal of Non-Newtonian Fluid Mechanics

journal homepage: www.elsevier.com/locate/jnnfm

# Predicting yielding in the pressure-driven flow of a Bingham fluid in a serpentine channel

T.G. Roberts[1], S.J. Cox *

*Department of Mathematics, Aberystwyth University, SY23 3BZ, UK*

ARTICLE INFO

*Keywords:*
Yield stress fluid
Serpentine channel
Finite element method
Foam sclerotherapy

ABSTRACT

The use of foams in applications such as enhanced oil recovery and varicose vein sclerotherapy has led to renewed interest in their flow as yield stress fluids. In each application one seeks to determine the ability of a foam to displace another fluid from a tortuous channel. We simulate the pressure-driven flow of a Bingham fluid through a serpentine two-dimensional channel to predict the effects of varying the channel geometry on the size and location of the unyielded regions in which the fluid is either stationary or moving as a plug. We discuss the implications for the effective displacement of blood in varicose vein sclerotherapy.

## 1. Introduction

Yield-stress fluids such as toothpaste [1], drilling mud [2], magma [3] and aqueous foam [4,5] are useful in many industrial and medical applications. A moving yield-stress fluid consists of unyielded, or plug, regions, which can be either static or moving depending on the local stresses and the channel geometry, surrounded by regions in which the stresses exceed the yield stress and the fluid flows. The existence of a yield stress means that the fluid resists mixing and can effectively displace another fluid. Conversely, the yield stress prevents fluid flow when applied forces are small [6] and hence makes some processes more difficult.

In enhanced oil recovery [7], for example, foam acts as a displacement fluid: unyielded regions of the foam have a large effective viscosity, which means that the foam can push the oil out of the formation, increasing the recovery factor. On the other hand, to move contaminated sludges [8] requires significant stresses to be applied and hence greater expenditure of energy.

Foam sclerotherapy is a minimally invasive treatment for varicose veins [4,9] in which a sclerosant-laden foam is used to displace stagnant blood from a varicose vein and to deliver sclerosant to the vein walls. The sclerosant kills the cells forming the veins' endothelial lining, which causes the vein to collapse. A foam with a high yield stress is used for the treatment, corresponding to a foam with a relatively low liquid fraction, because an extensive unyielded region improves the displacement of blood. Mixing of the foam with blood in the yielded regions close to the vein walls deactivates the sclerosant, providing a further benefit of a large plug region [9]. However, too high a yield stress makes it difficult to move the foam at all (as in the case of contaminated sludges), since the necessary pressure drop to induce flow would be high, making it difficult for the surgeon to squeeze the foam out of a syringe for injection into a vein. It is therefore worthwhile to predict the extent of the unyielded regions in a foam moving through a constricted channel, since this will allow the sclerotherapy process to be improved and optimised.

Previously we described the flow of an idealised yield-stress fluid, a Bingham fluid, in straight and uniformly curved channels [10]. To investigate the displacing capability of yield-stress fluids in more complex channel geometries, we present here the results of 2D finite element simulations of the pressure-driven flow of a Bingham fluid in a serpentine channel, relevant to applications such as well-drilling [11], residual drilling [12], pulsed cleaning [13], and delivery of toothpaste [14]. In this geometry (see Fig. 1), the direction of the fluid flow changes along the channel, providing insight into more realistic flows. We consider the effects of the magnitude of the yield-stress and the channel geometry on the position and extent of the unyielded regions within the channel.

The flow of Newtonian fluids has been investigated in a number of "corrugated" and "wavy" geometries, showing that secondary viscous eddies or flow reversal can occur when the amplitude of the corrugations is large [15–17]. The critical geometrical parameters which lead to secondary viscous eddies were determined numerically by Hemmat and Borhan [18] in a constricted channel.

When the fluid has a yield stress, the locations of the viscous eddies seen for Newtonian fluids broadly coincide with regions of static

* Corresponding author.
*E-mail address:* sxc@aber.ac.uk (S.J. Cox).
[1] Present address: Bangor University International College, Bangor, Gwynedd, LL57 2DG, UK.

https://doi.org/10.1016/j.jnnfm.2023.105131
Received 23 November 2022; Received in revised form 4 October 2023; Accepted 5 October 2023
Available online 10 October 2023

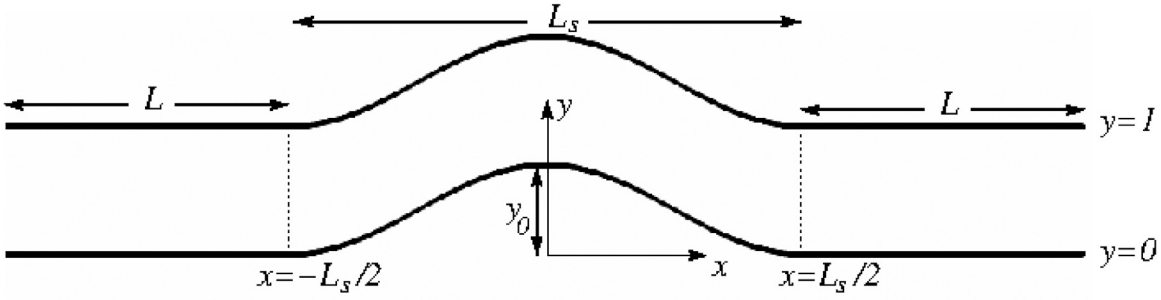


**Fig. 1.** The geometry of the channel, in which the shape of the central section is described by the sinusoidal function in Eq. (10). The height of the channel is fixed at $h = 1$ throughout, without loss of generality.

unyielded fluid. These "dead regions" [19,20] are situated at the walls of the channel and grow in size as the yield-stress increases and the amplitude of the channel increases [11,21]. For example, the plug of unyielded fluid located near the middle of the channel decreases in size at each bend of a sinusoidal-shaped channel [22], since the fluid stress increases there. Roustaei et al. [12] extend this to different shaped wavy channels, providing a "panorama" of images of the unyielded fluid regions in wavy channels, which are mostly confined to the peaks and troughs of the wall shape, as the yield stress and amplitude vary. The regions of stationary or dead fluid adjacent to the wall appear at approximately the same amplitude for all values of the yield stress. More recently, Rahmani and Taghavi [23] showed that it is possible to induce dead regions close to a flat wall by making the surface hydrophobic. Flows of yield stress fluids in channels with non-uniform width also include work on tapering channels [24–26], often using lubrication approximations to assist progress.

In the following we will quantify the critical channel wall amplitudes and yield stresses for the onset of dead regions in a particular collection of serpentine channels and quantify the size of the flowing and stationary plug regions relative to the total channel size.

## 2. Governing equations

We consider the flow of Bingham fluid through a sinusoidal channel to draw conclusions relevant, for example, to foam flow in veins during sclerotherapy.

In flows of this nature, we expect the Reynolds number to be small, of order $10^{-2}$ [27], since the foam is injected slowly into the vein to ensure a steady displacement of blood (e.g. 2.5 ml of foam injected over 15 s [28]). The relevant equations of motion are therefore the steady Stokes equations, and we neglect centripetal forces (Dean flow) [29]. Using $\tilde{}$ to denote dimensional variables, these are:

$$\underline{\tilde{\nabla}}.\underline{\underline{\tilde{\tau}}} = \underline{\tilde{\nabla}}\tilde{p}, \tag{1}$$

$$\underline{\tilde{\nabla}}.\underline{\tilde{u}} = 0. \tag{2}$$

The fluid flow-rate is determined in such a way [11,30] that the velocity in the straight part of the channel, leading towards and away from the sinusoidal part, is equal to the exact prediction [10] for a fluid with a given yield stress. The pressure gradient $\tilde{G}$ is defined as the difference between the inlet and outlet pressures divided by the total channel length $\tilde{L}_t$:

$$\underline{\tilde{\nabla}}\tilde{p} = \tilde{G} = \frac{\tilde{p}_{in} - \tilde{p}_{out}}{\tilde{L}_t}. \tag{3}$$

The length of the channel is discussed in more detail in Section 3. We will set $\tilde{p}_{out} = 0$ and find the appropriate value of $\tilde{p}_{in}$. The value of the inlet pressure required increases as the channel amplitude increases, as shown in Fig. 3(a). We apply no-slip boundary conditions to the walls of the channel.

The simplest constitutive equation for a yield-stress fluid is the Bingham model [31]. This has been studied extensively, including pioneering numerical investigations by Mitsoulis and co-workers, for example for channel flows [32], flow past a sphere [33] and a cylinder [34], and unsteady Couette flow [35].

The Bingham model is derived on the basis that if the magnitude of the fluid stress $|\underline{\underline{\tau}}|$ is less than the yield stress $\tilde{\tau}_0$, the strain-rate $\underline{\underline{\dot{\gamma}}}$ is zero and the resulting solid-like response inelastic. Here $|\underline{\underline{\tau}}| = \sqrt{\frac{1}{2}\left(\underline{\underline{\tau}} : \underline{\underline{\tau}}\right)}$ denotes the second invariant of the stress tensor (and similarly for the strain-rate tensor below). Above the yield stress, the relationship between stress and strain is linear.

For a fluid with (effective) viscosity $\tilde{\eta}$, the constitutive equation for this visco-plastic model takes the form

$$\underline{\underline{\tilde{\tau}}} = \left(\tilde{\eta} + \frac{\tilde{\tau}_0}{|\underline{\underline{\tilde{\dot{\gamma}}}}|}\right)\underline{\underline{\tilde{\dot{\gamma}}}} \qquad \text{for} \quad |\underline{\underline{\tilde{\tau}}}| \geq \tilde{\tau}_0 \tag{4}$$

$$\underline{\underline{\tilde{\dot{\gamma}}}} = \underline{\underline{0}} \qquad \text{for} \quad |\underline{\underline{\tilde{\tau}}}| < \tilde{\tau}_0.$$

We work with a dimensionless system of equations and characterise the yield stress behaviour with a Bingham number $B$. All lengths are normalised by the width of the channel, $\tilde{h}$, and $\tilde{U}$ denotes the mean fluid velocity. With a pressure-gradient $\tilde{G} = \tilde{\eta}\tilde{U}/\tilde{h}^2$ and time scale $\tilde{h}/\tilde{U}$, the constitutive equation becomes

$$\underline{\underline{\tau}} = \left(1 + \frac{B}{|\underline{\underline{\dot{\gamma}}}|}\right)\underline{\underline{\dot{\gamma}}} \qquad \text{for} \quad |\underline{\underline{\tau}}| \geq B \tag{5}$$

$$\underline{\underline{\dot{\gamma}}} = \underline{\underline{0}} \qquad \text{for} \quad |\underline{\underline{\tau}}| < B$$

where $B$ is defined as

$$B = \frac{\tilde{\tau}_0}{\tilde{G}\tilde{h}}. \tag{6}$$

The yield-stress of foams used in varicose vein sclerotherapy is of the order of a few Pascals [9,36].

For unidirectional flows in straight and annular channels [10,37,38] the relationship between stress and strain simplifies, which allows closed-form expressions for the velocity profile to be derived. In the more complex channel geometries that we consider here, numerical solution of the governing equations is required.

Simulations were performed with the finite element software, FreeFem++ [39], which solves the Stokes equations in weak form, with the velocities contained in finite element space P3 and the pressure in P1. The Bingham fluid is modelled as a generalised Newtonian fluid, as follows.

To avoid singularities at the yield surfaces in our numerical implementation we use the regularised Papanastasiou [40] viscosity model, which has previously been used to study Bingham fluids in many situations, including flow around obstacles [41,42], in channels with slip and/or non-slip boundary conditions [27,43]. The Papanastasiou

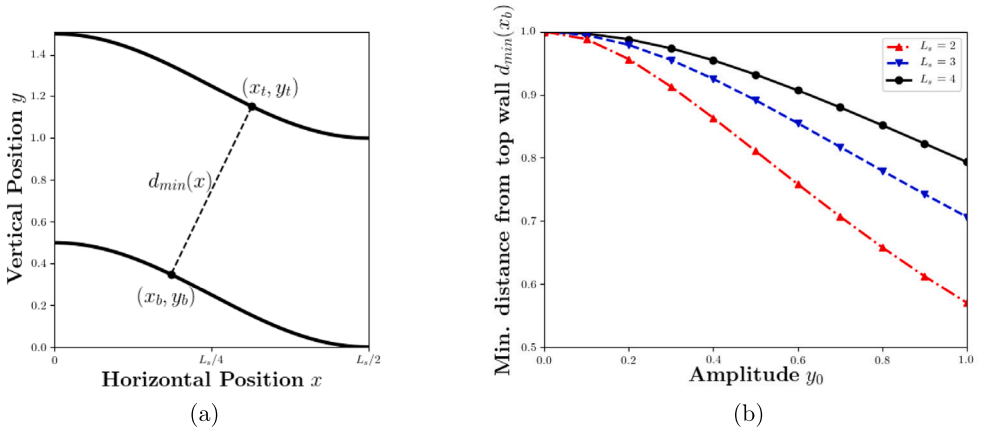


**Fig. 2.** (a) The location of the shortest distance $d_{min}(x)$ between the walls occurs part way along the curved part of the channel. Here $L_s = 3$ and $y_0 = 0.5$. (b) The shortest distance between the walls, defined as the minimum of $d(x_b)$ (Eq. (11)) decreases from the value in the straight part of the channel as the amplitude of the curved region increases.

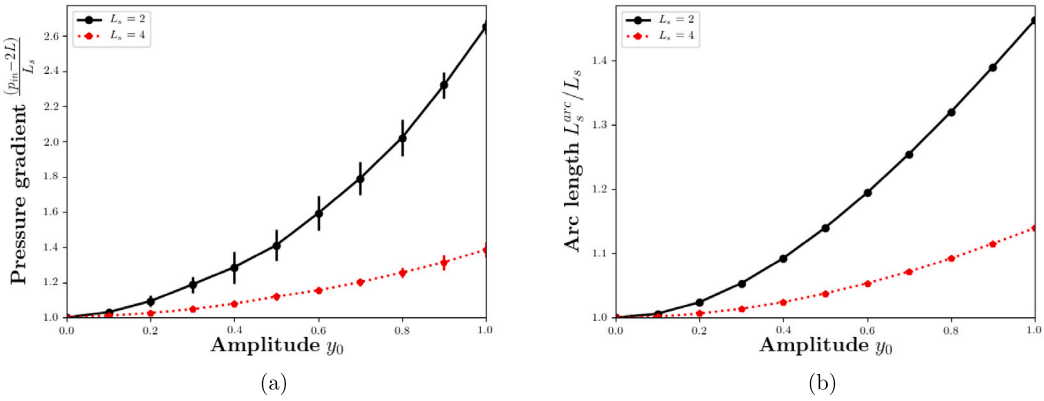


**Fig. 3.** (a) The calculated inlet pressure, $p_{in}$, required to maintain the expected velocity profile in the straight channel regions, expressed as a pressure gradient in the curved part of the channel. The contribution from the straight parts of the channel (of length $2L$) is subtracted to highlight the effects of channel curvature, indicating that the pressure exceeds the value that would be predicted on the basis of total arc length. Error bars indicate the small non-systematic variation between different values of the Bingham number. (b) The arc length of the curved part of the channel, scaled by $L_s$. Eq. (13) is evaluated for two values of the length of the curved part of the channel, $L_s$, for a range of values of the channel amplitude $y_0$. It is clear that as $L_s$ gets smaller, the effect on the arc length of the curvature of the channel is greater.

model [40] uses an exponential function to smooth the singularities that occur in Eq. (5), taking the form:

$$\underline{\underline{\tau}} = \left(1 + \frac{B}{|\underline{\underline{\dot{\gamma}}}|}\left(1 - \exp\left(-m|\underline{\underline{\dot{\gamma}}}|\right)\right)\right)\underline{\underline{\dot{\gamma}}}, \tag{7}$$

where $m$ is the regularisation parameter.

However, smoothing over the singularity at the yield stress leaves open the question of determining precisely the position of the yield surfaces [44], since the unyielded fluid is no longer a rigid solid but a "highly viscous fluid that approximates ideal viscoplastic behaviour" [45]. We use the following approximate (i.e. to leading order in $1/m$) criterion [44,46] to determine the critical (second invariant of the) strain rate $\delta$ at which the stress is equal to the yield stress, given in the form of a nonlinear equation:

$$m\delta = \log\left(\frac{B}{\delta}\right). \tag{8}$$

$\delta$ is therefore different for each choice of $m$ and $B$. With $m = 50{,}000$, we find that $\delta$ lies between $1.446 \times 10^{-4}$ and $1.692 \times 10^{-4}$ for $B$ in the range $0.2 - 0.8$, and is given approximately by:

$$\delta \approx 1.78 \times 10^{-5} \log(B) + 1.73 \times 10^{-4}. \tag{9}$$

The position of the yield surfaces are plotted by considering the logarithm of the second invariant of the strain rate $\log(|\underline{\underline{\dot{\gamma}}}|)$. Regions of fluid that experience a strain rate $|\underline{\underline{\dot{\gamma}}}| \leq \delta$ are considered to be unyielded. They are coloured in black in Figs. 4 and 5.

Each simulation commences with $B = 0$, thus solving the Stokes equations for a Newtonian fluid, and then the desired non-zero value of $B$ is introduced, allowing a profile of viscosity to develop over several hundred iterations according to Eq. (7). Our convergence criterion is that the sum of the velocities at each node of the mesh changes by less than $1 \times 10^{-5}$ between iterations. This was previously validated for flow in a uniformly curved channel, for which there is an analytical velocity profile [10]. The resolution of the finite element mesh within the sinusoidal region of the channel is greater than $2 \times 10^4$ nodes per unit area, which was the criterion for validating the accuracy of the numerical simulation in straight and curved channels [27].

In Section 3, we describe the channel geometry and highlight some additional factors to consider when varying the shape of the channel. We present the results of the simulations in Section 4, focusing on the shape and extent of the unyielded regions of the fluid. We summarise our conclusions, and the implications for processes such as sclerotherapy, in Section 5.

## 3. Channel geometry

We consider pressure-driven flow of a Bingham fluid through a channel of almost constant width that bends in first one direction then the other. The channel consists of two straight sections, the inflow and

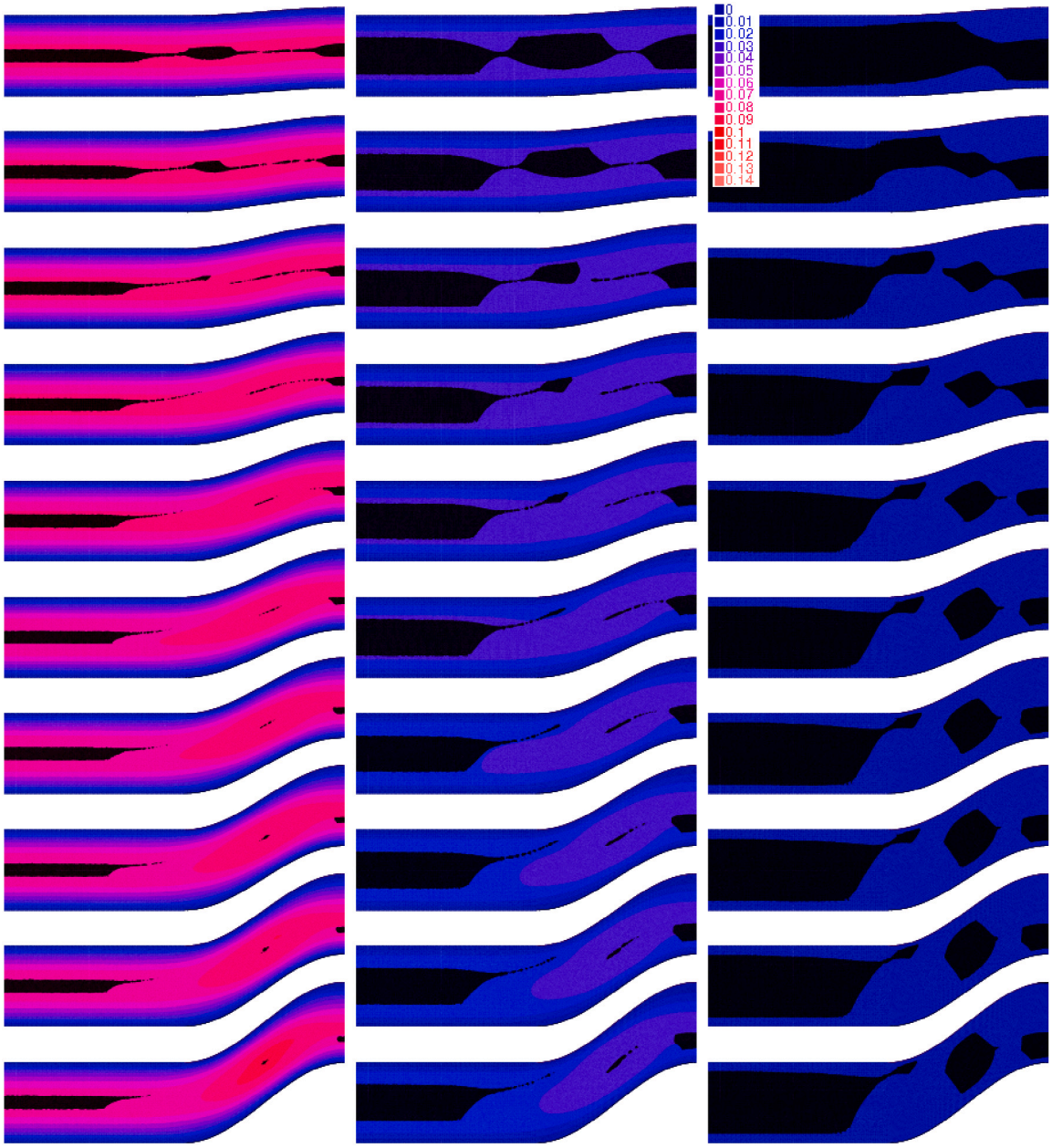


**Fig. 4.** Unyielded regions are shown in black and superimposed on contours of fluid speed for $L_s = 4$ for three values of the Bingham number $B = 0.2$ (first column), 0.5 (second column) and 0.8 (third column) and channel amplitudes $y_0$ increasing downwards, $y_0 = 0.1, 0.2, 0.3, \ldots, 1$. The pattern of yielding is symmetric about the line $x = 0$, so we show only the inlet half of the channel.

outflow regions, joined by a serpentine region of length $L_s$ defined by one period of a sinusoidal function. The deviation from the straight channel is measured by a parameter $y_0$ which we call the amplitude of the channel, taking values up to the channel width. Our coordinate system uses $x$ for the horizontal distance along the channel from its midpoint and $y$ as the vertical distance from the bottom channel wall, as shown in Fig. 1.

The straight inlet and outlet regions are of length $L$, chosen to be sufficiently large that any inflow and outflow effects occur far from the curved region. The lower wall of the curved part of the channel is given by the formula

$$y_l(x) = \frac{1}{2} y_0 \left( \cos\left( \frac{2\pi}{L_s} x \right) + 1 \right), \tag{10}$$

and the upper wall by $y_u(x) = y_l(x) + h$. The channel is symmetric about the line $x = 0$, with $|x| \le L_s/2$ referring to the curved part.

There are two subtleties associated with this channel geometry. The first is that although the vertical distance between the channel walls is fixed, the channel width (cf. Fig. 2) may be less than $h$ in places, and where it is less than $h$ it decreases with increasing amplitude $y_0$. That is, given a point $(x, y(x))$ on the top wall, the distance to the point $(x_b, y_b)$ at the foot of the perpendicular to the wall at $(x, y(x))$ is

$$d(x) = \sqrt{(x - x_b)^2 + (y_u(x) - y_l(x_b))^2} \tag{11}$$

$$= \sqrt{(x - x_b)^2 + \left( h + \frac{1}{2} y_0 \left( \cos\left( \frac{2\pi}{L_s} x \right) - \cos\left( \frac{2\pi}{L_s} x_b \right) \right) \right)^2}. \tag{12}$$

In Fig. 2(a) we show an example in which the minimum perpendicular distance between the walls is $d_{min} \approx 0.9$ for $L_s = 3$ and $y_0 = 0.5$. This decrease in the channel width near $x = \pm L_s/4$ implies that the flow rate will increase and that further yielding of the fluid is likely.

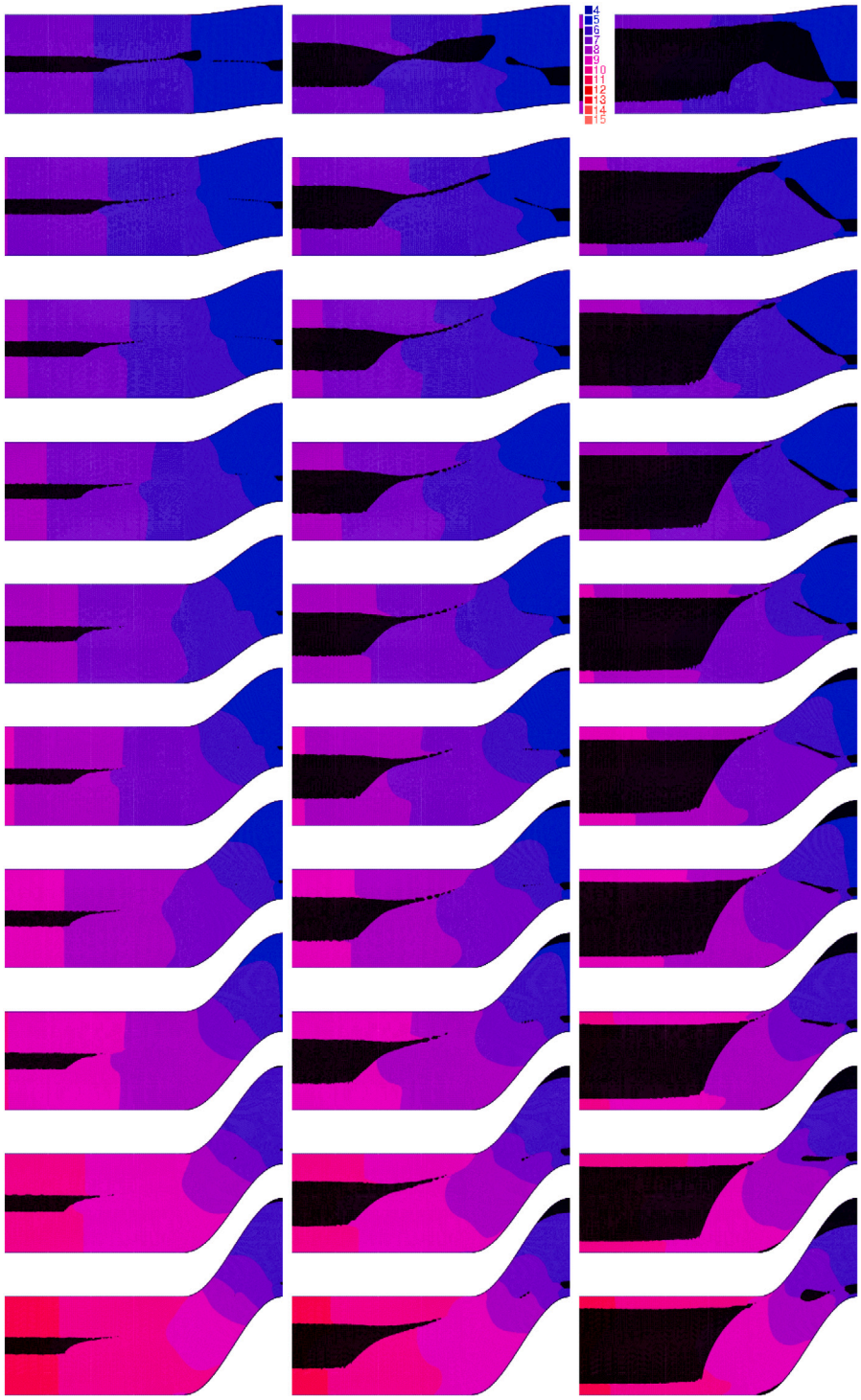

**Fig. 5.** Unyielded regions are shown in black and superimposed on contours of fluid pressure for $L_s = 2$ for three values of the Bingham number $B = 0.2$ (first column), 0.5 (second column) and 0.8 (third column) and channel amplitudes $y_0$ increasing downwards, $y_0 = 0.1, 0.2, 0.3, \ldots, 1$.

The second subtlety is that increasing the amplitude makes the channel longer. As a result, to maintain a given pressure gradient the inlet pressure must be increased if the amplitude is increased. The total channel length is $L_t = 2L + L_s^{arc}$, where

$$L_s^{arc}(y_0, L_s) = 2\int_0^{L_s/2} \sqrt{1 + (y'(x))^2}\, dx = 2\int_0^{L_s/2} \sqrt{1 + \left(y_0 \frac{\pi}{L_s} \sin\left(\frac{2\pi}{L_s}x\right)\right)^2}\, dx. \quad (13)$$

We evaluate the elliptic integral in Eq. (13) numerically, giving the values shown in Fig. 3(b).

## 4. Results

We consider values of $B$ between zero and one (since in a straight channel with unit pressure gradient the fluid becomes stationary when $B$ reaches one) and channel amplitudes $y_0$ between zero and one. The pressure gradient required to maintain the expected flow in the straight

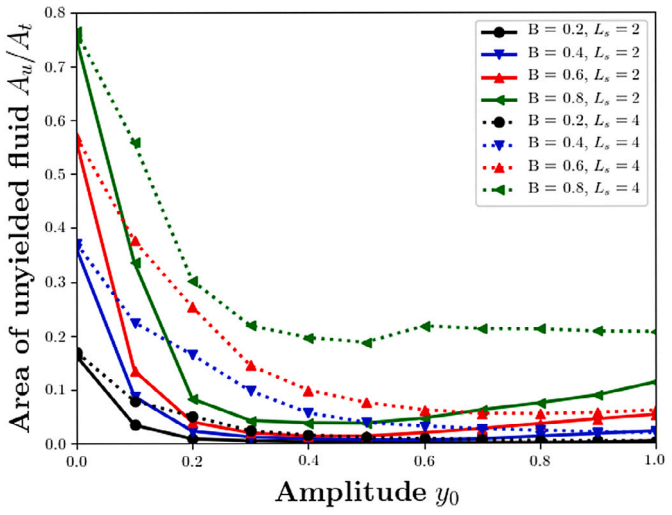


**Fig. 6.** The area of unyielded fluid $A_u$, relative to the curved channel area, decreases as the amplitude $y_0$ increases and decreases further with decreasing channel length $L_s$ (i.e. more tightly curved channels). The area of the dead regions $A_d$ increases with increasing amplitude and with decreasing channel length $L_s$, and is evident as a slight increase in unyielded area at larger $y_0$.

part of the channel (Fig. 3(a)) is greater than what would be predicted based only on the arc length of the channel (Fig. 3(b)). The discrepancy is due the changes in width of the channel, as described above, as well as the changes to the flow direction [47].

### 4.1. Location of unyielded regions

The pattern of unyielded fluid is shown in Fig. 4 for three different Bingham numbers, in the case where the curved part of the channel has length $L_s = 4$. At small Bingham number the yield surfaces lie close to the centre of the channel. Increasing the amplitude $y_0$ causes further yielding within the curved region, with the extent of this additional yielding dependent on $B$.

For small $y_0$ less than 0.3 there is little change in the position of the yield surfaces: the introduction of a small amount of channel curvature does not increase the stresses enough to cause all the fluid along the centre of the channel to yield. There is a slight thinning of the plug where the channel starts to curve away from the straight parts, and again around the peak of the sinusoid, but there remains a continuous plug along the centre of the channel [12].

At $y_0 = 0.3$, the unyielded region in the curved part of the channel becomes separated from the unyielded region in the straight parts of the channel (for all Bingham numbers), because of yielding close to the inlet/outlet of the curved region. The unyielded fluid in the straight parts of the channel retreats towards the inlet and outlet. The unyielded region in the curved part of the channel is displaced towards the inside of the bend at $x = 0$, because the fluid has a higher speed near the outer wall of the channel.

At $y_0 \approx 0.5$, the plug around $x = \pm L_s/4$ has almost completely disappeared for the two smaller Bingham numbers shown. For $B = 0.8$, on the other hand, diamond-shaped regions grow, almost completely spanning the channel. These can form because there is a pseudo-straight part of the channel forming here, for long channels with high amplitude.

For $y_0 \geq 0.8$ there is little change since most of the fluid in the curved part of the channel is yielded.

Fig. 4 also shows contours of velocity. As expected, the smaller the Bingham number, the larger the velocities, which approach the value $Gh^2/8\eta \approx 0.125$ for a Newtonian fluid in a straight channel. For given $B$, the maximum velocity grows with increasing channel amplitude $y_0$, which is more apparent at the smallest value of $B$ shown. The position of the maximum velocity moves away from $x = 0$ to around $x = \pm L_s/4$ with increasing amplitude (this is explored in detail for flow from a straight into a curved channel in [27]).

Fig. 5 shows a similar sequence of yield surfaces for a shorter channel ($L_s = 2$) with consequently greater curvature for given amplitude $y_0$. Hence there is much more yielding, and the plug regions are much smaller.

For $B = 0.2$ the region of unyielded fluid in the middle of the curved part of the channel separates from the unyielded fluid in the straight part of the channel for $y_0 \geq 0.1$, which is less than half the value in the case $L_s = 4$ (Fig. 4). The fluid in the curved region is almost entirely yielded at this small Bingham number.

For $B = 0.5$ and 0.8, thin fingers of unyielded fluid extend out from the plug in the inlet/outlet region and from the small region of unyielded fluid at $x = 0$. In the latter case, their orientation changes with increasing channel amplitude, pointing more directly up/downstream as $y_0$ increases.

Note also the static, or "dead", regions of fluid at the top wall of the channel at the highest amplitudes. These increase in size with increasing Bingham number, and are found at all amplitudes for $B = 0.8$. For this large $B$, there is a second, smaller, region of dead fluid on the other side of the channel where it first starts to curve.

Fig. 5 also shows contours of pressure, indicating how the pressure must increase in the inlet to maintain the width of unyielded region in the straight parts of the channel.

### 4.2. Area of yielded and unyielded fluid

In a straight channel, the area of the region of unyielded fluid per unit length is [27]:

$$A_u^{\text{str}} = B, \tag{14}$$

representing a strip of unyielded fluid in the centre of the channel, the width of which increases with $B$. This is visible on the left of Figs. 4 and 5.

The area of unyielded fluid in the curved part of the channel, $A_u$, is shown in Fig. 6 for different amplitudes $y_0$. $A_u$ is normalised by the total area of the curved part of the channel, $A_t$. As $y_0$ increases and the channel bends, $A_u/A_t$ decreases for all Bingham numbers $B$, starting from a value close to the straight-channel value (Eq. (14)), representing increased yielding. If the channel is more tightly curved (smaller $L_s$), $A_u$ reduces more quickly with $y_0$.

For the shorter channel, with $L_s = 2$, more than 80% of the fluid in the curved part of the channel yields for amplitudes $y_0 \geq 0.1$, and the curves saturate to a value below 0.2. For the longer channel, with $L_s = 4$, this threshold increases to about $y_0 \approx 0.3$, except for larger $B \geq 0.8$ where the curve saturates at about $A_u/A_t = 0.3$.

In some cases, either for large amplitude or small $L_s$, the fluid is almost completely yielded, even at intermediate amplitudes (cf. Fig. 5). Then as the amplitude increases further, we note the formation of dead regions, which we take to be those regions of the fluid that have stress below the yield stress and speed $|u| \leq 10^{-5}$, at the top of the curved part of the channel. This causes an increase in $A_u$, which we separate out, denoting the area of dead regions by $A_d$; this is shown later, in Fig. 9(a), and discussed in Section 4.2.2.

The area of the dead regions is greater for larger Bingham numbers and shorter, more curved, channels. Above a threshold in $y_0$, which increases with decreasing $B$, it increases almost linearly.

We therefore distinguish the areas of moving and stationary unyielded regions of fluid. We will give approximate fits to the data to provide simple estimates of the amount of unyielded and yielded fluid, and the amount of unmoving fluid.

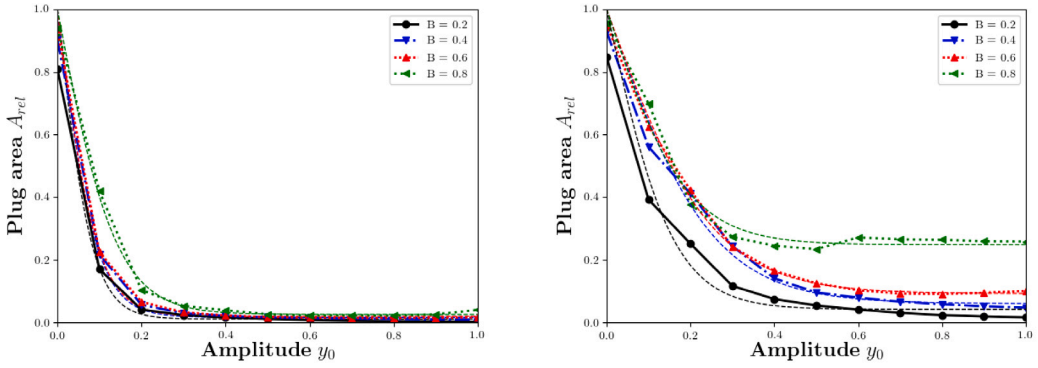


**Fig. 7.** The area of unyielded moving fluid $A_{rel}$, i.e. the plug area, relative to the curved channel area, decreases with the deviation from a straight channel (i.e. the amplitude $y_0$) for both channel lengths. It also increases at greater channel lengths $L_s$ (i.e. less-curved channels) for given amplitude, and is broadly similar for all values of the Bingham number $B$, particularly at small $L_s$. The dashed lines are fits to Eq. (16).

#### 4.2.1. Moving regions of unyielded fluid

For the moving plug of unyielded fluid, we record its area $A_p$ relative to the value expected in a straight channel:

$$A_{rel} = A_p / A_u^{\text{str}}. \tag{15}$$

For small $y_0$ we expect the relative area of unyielded fluid to be close to one, since the curvature is small. The value of $A_{rel}$ decreases with increasing amplitude $y_0$, as shown in Fig. 7, since more of the fluid yields as the channel curves and can reach values close to zero, indicating that the fluid yields everywhere.

As the length of the curved region decreases, the area of unyielded fluid decreases (Fig. 7(a)). The value of $A_{rel}$ at which the curves saturate as $y_0$ approaches 1 decrease towards zero for the smaller value of $L_s$, confirming that more of the fluid yields in more tightly curved channels. In addition, for smaller $L_s$ the differences between different values of $B$ become less noticeable.

The curves of $A_{rel}(y_0)$ in Fig. 7 are reminiscent of a hyperbolic tangent, with a straight line with finite slope followed by saturation to a constant value. We fit a tanh function to the data via two fitting parameters $A_0$ and $\epsilon_0$ to summarise the effects of the Bingham number $B$ and the channel length $L_s$ on yielding. The parameter $A_0$ measures the value at which $A_{rel}$ saturates for large $y_0$ and the parameter $\epsilon_0$ measures the effect of amplitude on yielding at smaller values of $y_0$. The fitting function takes the form:

$$A_{rel} = 1 - \left(1 - A_0(B, L_s)\right) \tanh\left(\frac{y_0}{\epsilon_0(B, L_s)}\right). \tag{16}$$

The values of parameters $A_0$ and $\epsilon_0$ are determined using non-linear least squares fitting in Python [48]; the values of the rms error of both parameters are very small, of the order $10^{-5}$ for $B \leq 0.7$. For $B = 0.8$ and $L_s = 4$, there is a notable discrepancy between the data and the fitting function, which results in a slightly higher error.

Fig. 8 shows the values of the fitted parameters. $\epsilon_0$, i.e. the degree of yielding with increasing $y_0$, is almost independent of the Bingham number for $B \leq 0.7$ and increases slightly with increasing channel length $L_s$. Its value increases sharply when $B$ gets close to one. To a reasonable approximation, the value of $\epsilon_0$ is constant, with

$$\epsilon_0 \approx 0.05 L_s. \tag{17}$$

Conversely $A_0$ increases with increasing $B$, but depends only weakly on the channel length. We assume a quadratic increase and make the approximation

$$A_0 \approx 0.1 \epsilon_0 L_s^2 B^2. \tag{18}$$

This is shown as grey dashed lines in Fig. 8. Then our empirical expression for the area of yielded fluid, caused by the curvature of the channel, relative to the result for a straight channel, is

$$A_{rel} \approx 1 - \left(1 - 0.005 L_s^3 B^2\right) \tanh\left(\frac{y_0}{0.05 L_s}\right). \tag{19}$$

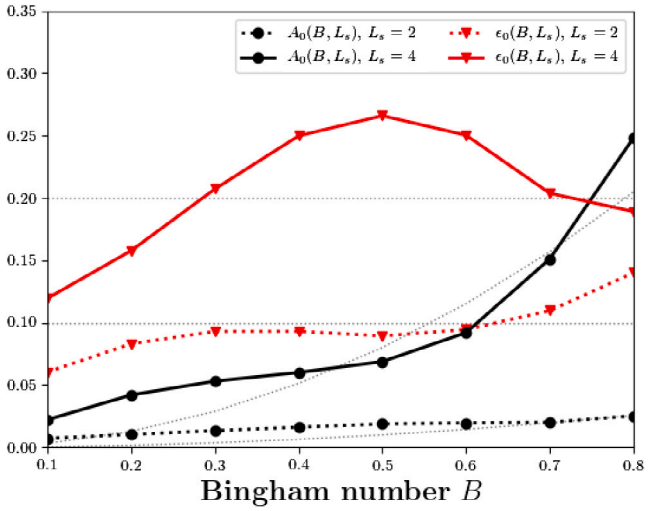


**Fig. 8.** The fitting parameters $A_0$ and $\epsilon_0$ for $A_{rel}(y_0)$ from Eq. (16) plotted as functions of the Bingham number $B$ for different channel lengths $L_s$. The error bars are smaller than the point size when plotted. Eqs. (17) and (18) are shown in grey for comparison with the fitting parameters.

#### 4.2.2. Dead regions of unyielded fluid

The dead regions are parts of the fluid in which the stress is below the yield stress and the fluid is not moving, always situated adjacent to the walls of the channel. To find an approximate form for the size of these regions, we fit the data for $L_s = 2$ in Fig. 9 using the linear function

$$A_d / A_t = C_0 \left(y_0 - D_0\right). \tag{20}$$

$C_0$ indicates how quickly the area of dead fluid increases with the amplitude of the channel, while $D_0$ is a measure of the amplitude at which dead regions start to form.

The fitted function is indicated by a dashed line on Fig. 9. As above, the parameters $C_0$ and $D_0$ are determined using non-linear least squares fitting in Python [49]. Again, the rms errors are small, of the order $10^{-5}$ for most values of $B$, increasing to $10^{-4}$ at $B = 0.9$ for the parameter $D_0$. Fig. 9(b) shows the values of the fitting parameters. $C_0$ increases almost linearly with increasing $B$:

$$C_0 \approx 0.15 B, \tag{21}$$

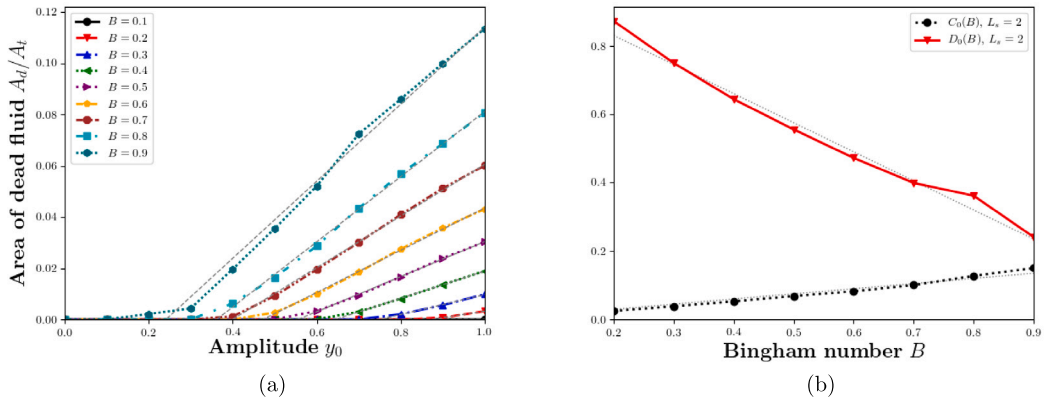


**Fig. 9.** (a) The area of dead fluid $A_d/A_t$ increases with the deviation from a straight channel (i.e. the amplitude $y_0$). The values are relatively large for $L_s = 2$, and negligible for the longer channel with $L_s = 4$. (b) The fit parameters $C_0$ and $D_0$ from Eq. (20) in the case $L_s = 2$. The ansatzes given in Eqs. (21) and (22) are shown as dashed lines.

while $D_0$ decreases almost linearly with $B$:

$$D_0 \approx 1 - 0.85B. \tag{22}$$

These fits are shown on Fig. 9.

Our rule of thumb for estimating the effect of channel curvature on the amount of dead fluid is therefore

$$A_d/A_t = 0.15B\left(y_0 + 0.85B - 1\right). \tag{23}$$

### 4.3. Velocity profiles

We determine the distribution of velocity in cross-sections of the channel at $x = -L_s/2$, the entrance to the curved region, and $x = 0$, the midpoint of the channel, at the top of the bend, and investigate how these profiles change with increasing amplitude $y_0$.

Fig. 10 shows the speed at both cross-sections for Bingham numbers $B = 0.2, 0.5$ and $0.8$ for $L_s = 2$. In the case $y_0 = 0$, the velocity profile in a straight channel has a horizontal part and two parabolic parts close to the walls, as expected. As the channel amplitude increases, the maximum speed at $x = 0$ increases (by at most 40%) (Fig. 10(a), (c) and (e)). The position of the maximum velocity moves towards the lower wall of the channel with increasing amplitude, as for the flow of a Bingham fluid in an annulus [10].

The profiles also show the extent of the dead regions that form at $x = 0$, which increase with increasing amplitude $y_0$ and Bingham number $B$. For $B = 0.8$ and $y_0 = 1$, the width of the dead region spans around 30% of the channel width.

In the cross-section at $x = -L_s/2$ (Fig. 10(b), (d) and (f)), the speed decreases with increasing channel amplitude as the fluid responds to the curvature of the channel. This becomes more evident as the Bingham number increases. The profiles confirm what is evident in Fig. 5, that even at small amplitudes the fluid becomes entirely yielded, since there are no longer straight parts to the velocity profile.

For the longer channel with $L_s = 4$ the trends in velocity are similar but less pronounced.

### 4.4. Pressure distribution

For a straight channel ($y_0 = 0$), the pressure decreases linearly with increasing position $x$, with fixed gradient $G = 1$. When the amplitude $y_0$ of the channel is non-zero, Fig. 5 shows that the pressure deviates from this linear profile.

We quantify this by recording the pressure along the centreline of the channel, $y = y_l(x) + h/2$ (cf. Eq. (10)), shown in Fig. 11. The pressure is antisymmetric about the centre of the channel ($x = 0$) so only the upstream half is shown. In the straight channel upstream from the entrance of the sinusoidal section, the gradient of pressure is similar for all amplitudes and Bingham numbers as expected (with $G = 1$), but the pressure itself increases with the length and curvature of the sinusoidal part of the channel.

As the end of the straight part of the channel is approached there is a drop in pressure, which is more abrupt for a shorter channel and higher Bingham number. Within the curved part of the channel the pressure gradient is almost constant again. In this region there is only a weak effect of Bingham number on the pressure, and the precise channel geometry is more significant.

## 5. Discussion

We have investigated the pressure-driven flow of a model yield-stress fluid at different Bingham numbers $B$ through serpentine channels with different amplitudes $y_0$ and lengths $L_s$, and illustrated the effect of these parameters on the extent to which the fluid yields. As the amplitude of the channel increases, the width of the channel decreases and, by conservation of mass, we expect the flow rate to increase: this increases the amount of yielded fluid, quantified relative to the expected area of yielded fluid in a straight channel. Similarly, reducing the length of the curved section of the channel, and effectively increasing the curvature of the walls, leads to more yielding.

We give rules of thumb (Eqs. (19) and (23)) for the extra yielding that is caused by the curvature of the channel, over and above the value expected for a straight channel, and for the size and onset of the dead regions of stationary, unyielded, fluid.

For the purpose of varicose vein sclerotherapy, quantifying the size of the moving plug regions and the dead regions is important as it is a direct indication of where, and the extent to which, the process is failing. As shown in Fig. 4, yielding, even at small $y_0$, could lead to additional mixing of the two fluids, in this example foam and blood, and hence the deactivation of the sclerosant.

The size of the moving plug regions, $A_{rel}$, is a measure of the effectiveness of a yield stress fluid in displacing a second fluid. Keeping the value of $A_{rel}$ as large as possible is beneficial, since having more fluid moving in a plug would improve the capability of the yield stress fluid to displace another fluid. Fig. 7(b) shows that a large Bingham number, and hence a large yield-stress, is good. On the other hand, in strongly-curved channels a large Bingham number increases the size of the dead regions, where no motion occurs, emphasising the need to keep the channel, or the vein, as straight as possible [10]. Straightening the channel, or vein, i.e. decreasing the amplitude $y_0$ and/or increasing the length $L_s$, would allow larger regions of unyielded fluid to move through the vein, leading to a more effective displacement of blood and delivery of surfactant to the endothelial cells.

For large values of the Bingham number $B$ the fluid may become stationary everywhere. In a straight channel, the critical value of $B$ at which this happens is one. We expect the critical value of $B$ at which

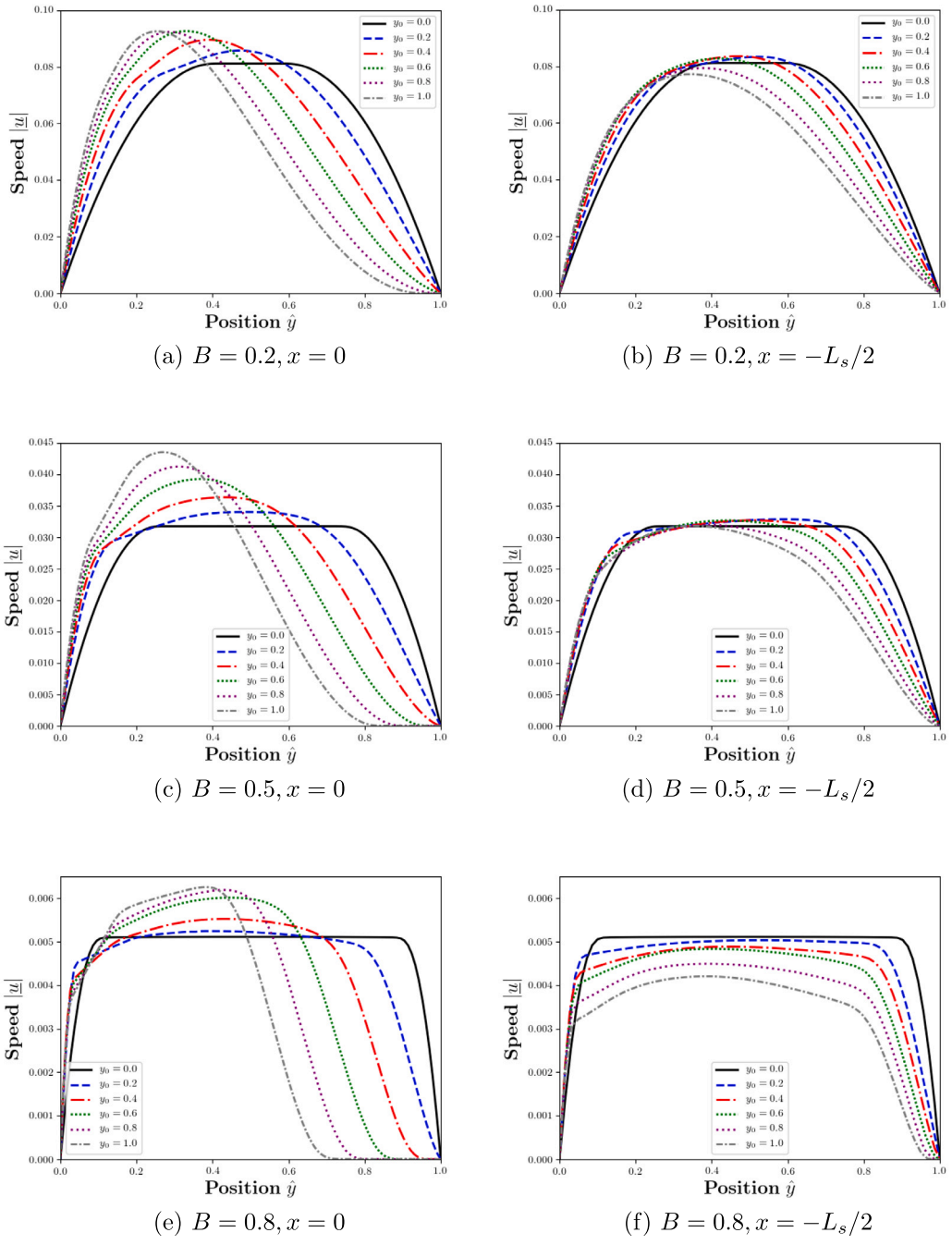


**Fig. 10.** Velocity profiles at cross-sections $x = 0$ and $x = -L_s/2$ for the case $L_s = 2$ showing the deviation from the symmetric profile seen in the straight channel case as the amplitude $y_0$ increases. The maximum velocity increases at $x = 0$ with increasing amplitude whereas the speed decreases almost everywhere at $x = -L_s/2$.

fluid flow ceases to decrease as the curvature increases [10]. Due to our use of a straight inlet and outlet section to the channel, motivated by the application to sclerotherapy, we are unable to determine the critical value of the Bingham number at which the flow becomes stationary in a purely sinusoidal channel. Such a calculation might be performed using periodic boundary conditions on the ends of the channel, and this is something that we will consider in future work.

## Declaration of competing interest

The authors declare the following financial interests/personal relationships which may be considered as potential competing interests: SJ Cox reports financial support was provided by Engineering and Physical Sciences Research Council. TG Roberts reports financial support was provided by BTG plc.

## Data availability

Data will be made available on request.

## Acknowledgements

We acknowledge financial support from the UK Engineering and Physical Sciences Research Council (EP/N002326/1) and a Ph.D. studentship from BTG.

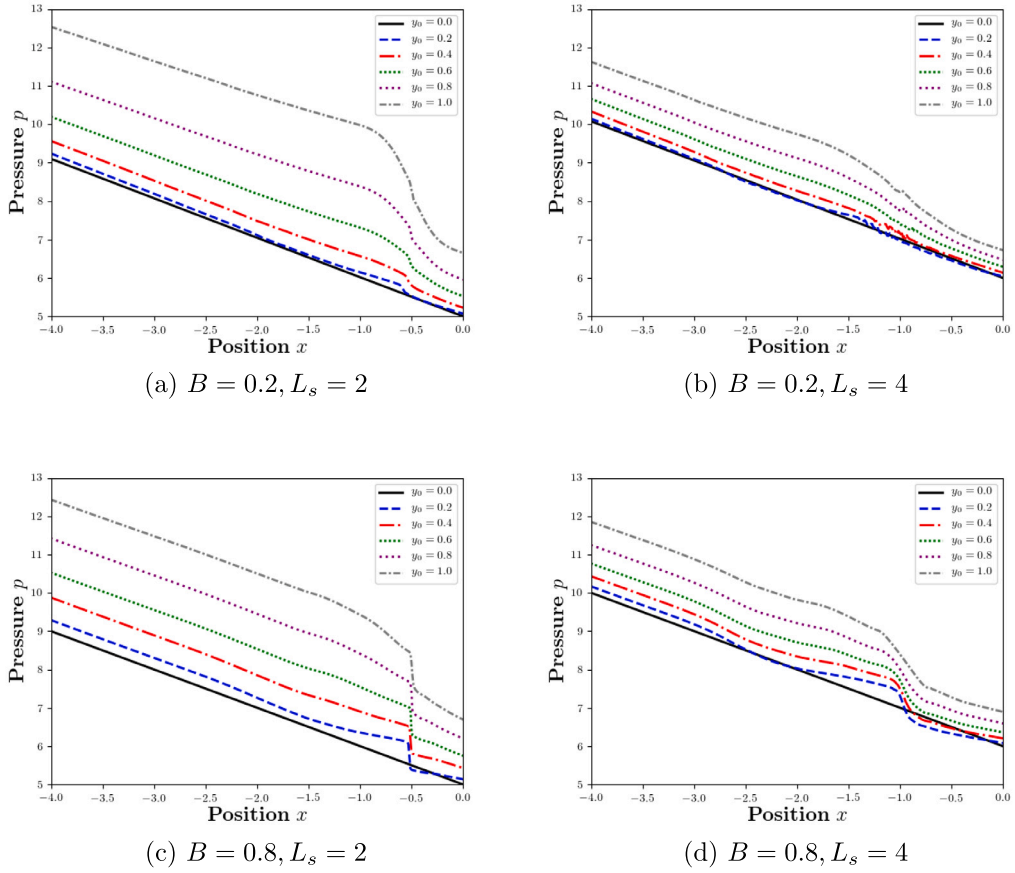


(a) $B = 0.2, L_s = 2$ (b) $B = 0.2, L_s = 4$

(c) $B = 0.8, L_s = 2$ (d) $B = 0.8, L_s = 4$

**Fig. 11.** The pressure $p$ along the channel centreline for two values of the Bingham number $B$ and channel lengths $L_s$. Values are shown from part-way along the straight inlet region to the centreline of the channel, $x = 0$, since the pressures are antisymmetric about the latter point.

## References


[1] I. Cantat, S. Cohen-Addad, F. Elias, F. Graner, R. Höhler, O. Pitois, F. Rouyer, A. Saint-Jalmes, Foams: Structure and Dynamics, OUP Oxford, 2013.

[2] H.A. Barnes, J.F. Hutton, K. Walters, An Introduction to Rheology, Elsevier, Oxford, 1989.

[3] S.D. Walsh, M.O. Saar, Magma yield stress and permeability: Insights from multiphase percolation theory, J. Volcanol. Geotherm. Res. 177 (4) (2008) 1011–1019.

[4] V. Nastasa, K. Samaras, Ch. Ampatzidis, T.D. Karapantsios, M.A. Trelles, J. Moreno-Moraga, A. Smarandache, M.L. Pascu, Properties of polidocanol foam in view of its use in sclerotherapy, Int. J. Pharm. 478 (2015) 588–596.

[5] I. Cantat, R. Delannay, Dynamical transition induced by large bubbles in two-dimensional foam flows, Phys. Rev. E 67 (3) (2003) 031501.

[6] B.S. Gardiner, B.Z. Dlugogorski, G.J. Jameson, R.P. Chhabra, Yield stress of firefighting foams, in: Proc. Halon Options Technical Working Conference, Albuquerque, New Mexico, 1998, pp. 12–14.

[7] R. Farajzadeh, A. Andrianov, R. Krastev, G.J. Hirasaki, W.R. Rossen, Foam-oil interaction in porous media: implications for foam assisted enhanced oil recovery, Adv. Colloid. Interfaces 183 (2012) 1–13.

[8] F. Yang, A. Bick, S. Shandalov, A. Brenner, G. Oron, Yield stress and rheological characteristics of activated sludge in an airlift membrane bioreactor, J. Membr. Sci. 334 (1–2) (2009) 83–90.

[9] T.G. Roberts, S.J. Cox, A.L. Lewis, S.A. Jones, Characterisation and optimisation of foams for varicose vein sclerotherapy, Biorheology 57 (2–4) (2021) 77–85.

[10] T.G. Roberts, S.J. Cox, An analytic velocity profile for pressure-driven flow of a Bingham fluid in a curved channel, J. Non-Newton. Fluid Mech. (2020) 104278.

[11] A. Roustaei, I.A. Frigaard, The occurrence of fouling layers in the flow of a yield stress fluid along a wavy-walled channel, J. Non-Newton. Fluid Mech. 198 (2013) 109–124.

[12] A. Roustaei, A. Gosselin, I.A. Frigaard, Residual drilling mud during conditioning of uneven boreholes in primary cementing. part 1: Rheology and geometry effects in non-inertial flows, J. Non-Newton. Fluid Mech. 220 (2015) 87–98.

[13] G.K. Christian, P.J. Fryer, The effect of pulsing cleaning chemicals on the cleaning of whey protein deposits, Food Bioprod. Process. 84 (4) (2006) 320–328.

[14] P.A. Cole, K. Asteriadou, P.T. Robbins, E.G. Owen, G.A. Montague, P.J. Fryer, Comparison of cleaning of toothpaste from surfaces and pilot scale pipework, Food Bioprod. Process. 88 (4) (2010) 392–400.

[15] J.L. Higdon, Stokes flow in arbitrary two-dimensional domains: shear flow over ridges and cavities, J. Fluid Mech. 159 (1985) 195–226.

[16] B.R. Munson, A.A. Rangwalla, J.A. Mann III, Low Reynolds number circular Couette flow past a wavy wall, Phys. Fluids 28 (9) (1985) 2679–2686.

[17] C. Pozrikidis, et al., Boundary Integral and Singularity Methods for Linearized Viscous Flow, Cambridge University Press, 1992.

[18] M. Hemmat, A. Borhan, Creeping flow through sinusoidally constricted capillaries, Phys. Fluids 7 (9) (1995) 2111–2121.

[19] P.O. Brunn, B. Abu-Jdayil, Axial annular flow of plastic fluids: Dead zones and plug-free flow, Rheol. Acta 46 (4) (2007) 449–454.

[20] I.A. Frigaard, K.G. Paso, P.R. de Souza Mendes, Bingham's model in the oil and gas industry, Rheol. Acta 56 (3) (2017) 259–282.

[21] N.J. Balmforth, R.V. Craster, D.R. Hewitt, S. Hormozi, A. Maleki, Viscoplastic boundary layers, J. Fluid Mech. 813 (2017) 929–954.

[22] A. Roustaei, Yield Stress Fluid Flows in Uneven Geometries: Applications to the Oil & Gas Industry (Ph.D. thesis), University of British Columbia, 2016.

[23] H. Rahmani, S.M. Taghavi, Poiseuille flow of a Bingham fluid in a channel with a superhydrophobic groovy wall, J. Fluid Mech. 948 (2022) A34.

[24] L. Fusi, K.D. Housiadas, G.C. Georgiou, Flow of a Bingham fluid in a pipe of variable radius, J. Non-Newton. Fluid Mech. 285 (2020) 104393.

[25] L. Fusi, A. Farina, Flow of a Bingham fluid in a non symmetric inclined channel, J. Non-Newton. Fluid Mech. 238 (2016) 24–32, Viscoplastic Fluids From Theory to Application 2015 (VPF6).

[26] L. Fusi, A. Farina, F. Rosso, Flow of a Bingham-like fluid in a finite channel of varying width: A two-scale approach, J. Non-Newton. Fluid Mech. 177–178 (2012) 76–88.

[27] T.G. Roberts, Modelling Foam Flow Through Vein-Like Geometries (Ph.D. thesis), Aberystwyth University, 2020, https://pure.aber.ac.uk/portal/files/42991428/Roberts_Tirion.pdf.

[28] A.W. Bradbury, G. Bate, K. Pang, K.A. Darvall, D.J. Adam, Ultrasound-guided foam sclerotherapy is a safe and clinically effective treatment for superficial venous reflux, J. Vasc. Surg. 52 (4) (2010) 939–945.

[29] W. Dean, Fluid motion in a curved channel, Proc. R. Soc. Lond. Ser. A Math. Phys. Eng. Sci. 121 (1928) 402–420.

[30] D.R. Hewitt, M. Daneshi, N.J. Balmforth, D.M. Martinez, Obstructed and channelized viscoplastic flow in a Hele–Shaw cell, J. Fluid Mech. 790 (2016) 173–204.
[31] E.C. Bingham, Fluidity and Plasticity, Vol. 2, McGraw-Hill, New York, 1922.
[32] S.S. Abdali, E. Mitsoulis, N.C. Markatos, Entry and exit flows of Bingham fluids, J. Rheol. 36 (2) (1992) 389–407.
[33] J. Blackery, E. Mitsoulis, Creeping motion of a sphere in tubes filled with a Bingham plastic material, J. Non-Newton. Fluid Mech. 70 (1997) 59–77.
[34] E. Mitsoulis, On creeping drag flow of a viscoplastic fluid past a circular cylinder: wall effects, Chem. Eng. Sci. 59 (4) (2004) 789–800.
[35] L. Muravleva, E. Muravleva, G.C. Georgiou, E. Mitsoulis, Unsteady circular couette flow of a Bingham plastic with the augmented Lagrangian method, Rheol. Acta 49 (2010) 1197–1206.
[36] A. Meghdadi, S.A. Jones, V.A. Patel, A.L. Lewis, T.M. Millar, D. Carugo, Foam-in-vein: A review of rheological properties and characterization methods for optimization of sclerosing foams, J. Biomed. Mater. Res. B Appl. Biomater. 109 (1) (2021) 69–91.
[37] R.B. Bird, G.C. Dai, B.J. Yarusso, The rheology and flow of viscoplastic materials, Rev. Chem. Eng. 1 (1983) 1–70.
[38] E. Sutton, A. Juel, A. Kowalski, C.P. Fonte, Dynamics and friction losses of the flow of yield-stress fluids through 90° pipe bends, Chem. Eng. Sci. 251 (2022).
[39] F. Hecht, New developments in FreeFem++, J. Numer. Math. 20 (3–4) (2012) 251–266.
[40] T.C. Papanastasiou, Flows of materials with yield, J. Rheol. 31 (5) (1987) 385–404.
[41] A. Mehmood, R. Mahmood, A.H. Majeed, F.J. Awan, Flow of the Bingham-papanastasiou regularized material in a channel in the presence of obstacles: correlation between hydrodynamic forces and spacing of obstacles, Model. Simul. Eng. 2021 (2021) 1–14.
[42] A. Franci, X. Zhang, 3D numerical simulation of free-surface Bingham fluids interacting with structures using the PFEM, J. Non-Newton. Fluid Mech. 259 (2018) 1–15.
[43] P. Panaseti, G.C. Georgiou, Viscoplastic flow development in a channel with slip along one wall, J. Non-Newton. Fluid Mech. 248 (2017) 8–22.
[44] A. Putz, I.A. Frigaard, D.M. Martinez, On the lubrication paradox and the use of regularisation methods for lubrication flows, J. Non-Newton. Fluid Mech. 163 (1–3) (2009) 62–77.
[45] G.R. Burgos, A.N. Alexandrou, V. Entov, On the determination of yield surfaces in Herschel–Bulkley fluids, J. Rheol. 43 (3) (1999) 463–483.
[46] I.A. Frigaard, C. Nouar, On the usage of viscosity regularisation methods for viscoplastic fluid flow computation, J. Non-Newton. Fluid Mech. 127 (1) (2005) 1–26.
[47] F. Danane, A. Boudiaf, O. Mahfoud, S.E. Ouyahia, N. Labsi, Y.K. Benkahla, Effect of backward facing step shape on 3d mixed convection of Bingham fluid, Int. J. Therm. Sci. 147 (2020) 106116.
[48] P. Virtanen, R. Gommers, T.E. Oliphant, M. Haberland, T. Reddy, D. Cournapeau, E. Burovski, P. Peterson, W. Weckesser, J. Bright, et al., Scipy 1.0: fundamental algorithms for scientific computing in python, Nature Methods 17 (3) (2020) 261–272.
[49] Scipy.org. Curve fit - python, 2020, https://docs.scipy.org/doc/scipy/reference/generated/scipy.optimize.curve_fit.html, [Online; accessed 05-May-2020].